

Modeling Ice Friction for Vehicle Dynamics of a Bobsled with Application in Driver Evaluation and Driving Simulation*

Julian von Schleinitz^{1,*}, Lukas Wörle¹, Michael Graf², Andreas Schröder³

Abstract

We provide an ice friction model for vehicle dynamics of a two-man bobsled which can be used for driver evaluation and in a driver-in-the-loop simulator. Longitudinal friction is modeled by combining experimental results with finite element simulations to yield a correlation between contact pressure and friction. To model lateral friction, we collect data from 44 bobsleigh runs using special sensors. Non-linear regression is used to fit a bob-specific one-track vehicle dynamics model to the data. It is applied in driving simulation and enables a novel method for bob driver evaluation. Bob drivers with various levels of experience are investigated. It shows that a similar performance of the top drivers results from different driving styles.

Keywords: Ice Friction, Bobsleigh, Driver Evaluation, Vehicle Dynamics

1. Introduction

In the sport of bobsleigh, the driver, the bobsled and especially the interaction between both are a crucial part of the overall performance. A key element in understanding this system is the friction between the runners and the ice surface. The friction of steel on ice is very low, enabling the possibility of fast wintersports like luge, bobsleigh or skeleton reaching top speeds of over 150kph. However, the ultra low friction of ice arises from complex material behavior and is a matter of current research [1]. Therefore, specific experiments and simulations are important to make further advances in this science area and to enable performance improvements in winter sports.

Most experiments are carried out under simplified conditions (see Section 1.1) compared to a highly dynamic bob run on a track. In particular, the lateral friction of a bob runner, which occurs when the velocity vector of the runner does not align with its longitudinal axis, is often not considered. This is surprising given that lateral friction is approximately one order of magnitude higher than the longitudinal friction and has significant implications on athlete and bobsled performance. In general, vehicle dynamics in combination

*This work was generously supported by BMW AG.

*Corresponding author

¹BMW AG

²Graf Engineering

³University of Salzburg

with ice friction is sparsely researched. This work aims to close this gap by providing a friction model for a bobsled with application in the area of driver evaluation and driving simulation.

The friction model is created and validated with real-world measurement data. In the case of lateral friction, which is crucial for realistic driving behavior in a simulator, the data originates from measurements with a professional bobsled suited for international competitions under race conditions. Our generated friction model is implemented at the BMW bobsled simulator which is being used by the German bobsleigh national team for preparation for the 2022 Olympic Winter Games.

1.1. Related work

1.1.1. Longitudinal friction

The majority of research for steel-ice friction focuses on longitudinal friction, i.e. the frictional force which acts against the driving direction. There are different kinds of experimental setups to investigate ice friction. For example, Hainzmaier [2] utilized an iced centrifuge with a slider gliding over a flat surface. Scherge et al. [3] used a modified tire test bench, where the slider glides in a concave curvature and determined a range for the longitudinal friction coefficient $\mu_x = 7 - 16 \cdot 10^{-3}$. Scherge et al. [4] also tested the influence of speed and temperature and found a lower limit for the friction coefficient $\mu_x \geq 8 \cdot 10^{-3}$ under their experimental conditions. Unlike rotational devices, linear devices are better suited to investigate ice friction on a fresh surface [1]. Makkonen and Tikanmäki [5] also pointed out that devices where a slider repeatedly glides over the same surface could lead to misinterpretation due to frictional heating. Hasler et al. [6] conducted ski-sport specific tests on a 24m linear tribometer. It was also used to optimize luge steels for the Austrian luge national team.

Real-life experiments are closely correlated to the application area. de Koning et al. [7] provided friction coefficients for speed skating by utilizing strain gauges ($\mu_x = 4.6 - 5.9 \cdot 10^{-3}$). Poirier et al. [8] investigated ice friction on a bobsleigh track during a bob race with a radar gun ($\mu_x = 3.6 - 5.3 \cdot 10^{-3}$). They performed friction experiments in an ice house as well ($\mu_x = 4.2 \cdot 10^{-3}$) [9]. Irbe et al. [10] performed tests with a skeleton at the start ramp of a track ($\mu_x = 4.3 - 6.72 \cdot 10^{-3}$). Lozowski et al. [11] developed a numerical model for longitudinal friction of a bobsled runner and compared different runner geometries on a flat surface and determined $\mu_x \approx 4.6 - 4.8 \cdot 10^{-3}$ for rocker radii (i.e. radii of the runners in longitudinal direction) between 20 and 50m and cross section radii from 4-7mm. All these real-life experiments were only carried out on straight sections of a track. An exception is Mössner et al. [12] who determined $\mu_x = 10 - 12 \cdot 10^{-3}$ for luge on the track in Vancouver, which is substantially higher than the other real life experiments.

While the above mentioned studies show significant deviations and were not executed under the same conditions, most real life experiments for bobsleigh are located at around $\mu_x \approx 4 \cdot 10^{-3}$.

An important factor of influence on ice friction is the contact pressure which is exerted on the ice by the gliding material [2]. Hainzmaier [2] reported a pressure dependency of the longitudinal friction coefficient. Lieferink et al. [13] also stated that pressure, temperature and speed have an important impact on ice friction, which is confirmed by Velkavrh et al. [14]. Unlike ice temperature, gliding speed or normal force, the pressure

which is exerted on the ice can be influenced by altering the contact area of the bobsled runners, making it a very important parameter in practice. This is supported by the considerable effort that bob teams around the world put into optimizing the shape of bobsled runners.

1.1.2. Lateral friction

Literature investigating the lateral friction of a bobsled is sparser even though it is much more important for its driving behavior. Most studies were conducted in the context of a bob simulator or simulation model. Rempfler [15] developed a bob simulator and found a lateral friction coefficient of $\mu_y = 0.02 - 0.1$ to reproduce realistic driving behavior in the simulator, which is also described in [16]. Arnold [17] calculated an upper bound for the lateral friction coefficient based on results provided by Hainzmaier [2] with $\mu_y \leq 0.11 - 0.28$. According to Scherge [18], the lateral friction for a bobsled is ten times higher than longitudinal friction, which would account for $\mu_y = 0.05 - 0.09$. Braghin et al. [19] developed a bob driver model for bobsled optimization and provided an equation for the lateral friction force F_y based on the normal force F_z and the side slip angle of the runner α

$$F_y = \mu_y F_z \frac{2}{\pi} \text{atan}(k_3 \alpha), \quad (1)$$

whereby it holds for the parameter $k_3 = 50 \text{rad}^{-1}$ and $\mu_y = 0.5$ [20]. It seems that they used this equation for both front and rear axle. To sum up, the friction coefficients reported in literature seem to be highly dependent on the experimental circumstances, as the deviations are quite high. We believe that a certain amount of the deviations can be explained by a combination of lateral and longitudinal friction. Especially, when determining friction on a track where lateral friction is needed to achieve the desired trajectory, combined friction needs to be accounted for, e.g. by using a dynamic vehicle model. This may be an explanation as to why the friction coefficient reported by Mössner et al. [12] is so high: it is an average over a complete track and therefore also includes the contribution of lateral friction.

1.1.3. Driver evaluation

The research into bob driver evaluation is a field with very few publications. This is interesting since there is high potential for performance improvements for both athlete and bobsled development. In contrast, in motorsport considerable effort is put into adjusting the setup of a race car to the driver's driving style [21, 22, 23], with driving simulators also being used for that task [24, 25]. von Schleinitz et al. [26] presented a method for race driver evaluation using a tire grip potential exploitation rating, i.e. it was analyzed how much of the available grip was utilized by the driver. The method we present is similar in some sense. Since bob drivers cannot actively accelerate in the driving direction, the best they can do is to minimize the frictional losses.

Though, not directly intended for driver evaluation, there are some works dealing with simulation models which could be used for that task. For example Gong et al. [27] created a simple steering model for a skeleton simulation and analyzed different control strategies. Zhang et al. [28] developed steering models for bobsleigh using optimal control. However, for both cases, a virtual model of a track has to be created, therefore it is not

possible to directly evaluate drivers using only real world data.

1.2. Overview

The rest of this work is structured as follows. Section 2 details the materials and methods. The aim is develop a model for both longitudinal and lateral friction. First, the data acquisition hardware is described. A friction experiment in an ice house is carried out to determine the longitudinal friction coefficient for various samples. We use a finite element contact simulation to obtain the contact pressure which is exerted on the ice. Both results are combined to an equation for the longitudinal friction force. Then, we create a bob-specific one-track model to describe its vehicle dynamics. Using data measured on a bob track, non-linear regression is utilized to fit a lateral friction model for the front and rear runner. The application of the friction model for a driving simulator is briefly sketched. What is more, the model is used to evaluate bob drivers by comparing the calculated energy losses caused by ice friction and also aerodynamic drag. The key element is that both losses depend on the angle of the runner or the bob itself to the driving direction and can therefore be influenced by the driver.

Section 3 presents the results of this study. Parameters for the longitudinal and lateral friction model are shown and the vehicle dynamics model is validated and compared to another model from literature. Lastly, the driver evaluation method is applied to analyze five bob drivers with various levels of experience.

Summarized, the main contributions of this work are: (1) A bob-suitable vehicle dynamics model for driving simulation which is real-time executable and can be used for analyzing ice friction. (2) A novel method for bob driver evaluation using real world measurement data. (3) Application of the driver evaluation method on a data set containing different drivers showing that different driving styles results in a similar overall performance.

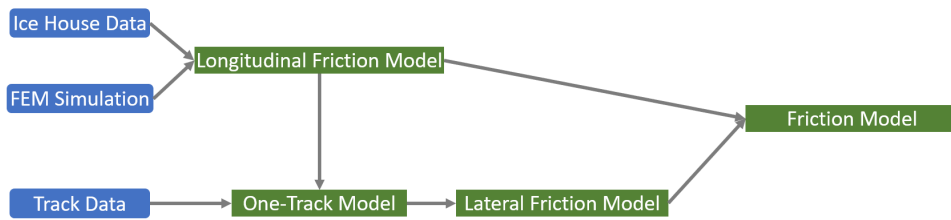
2. Materials and methods

2.1. Data acquisition

In this paper we used measurement devices from automotive applications which are common in motorsport. Table 3 lists the sensors and the measured quantities. The sample rate was between 100 and 500Hz depending on the sensor. The data was filtered using a low-pass filter and afterwards downsampled to 100Hz for further analysis. The symbols and subscripts used in this paper are listed in Table 2 and Table 1, respectively.

2.2. Longitudinal friction model

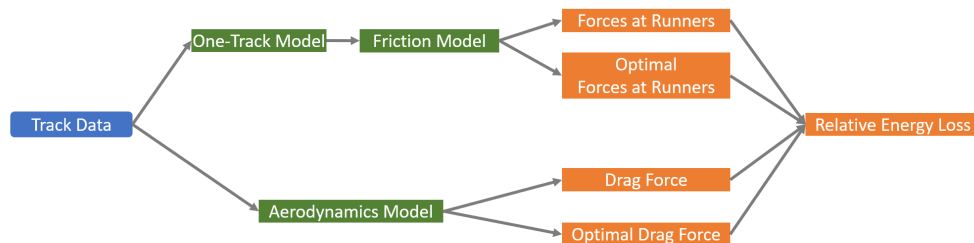
Measuring the ultra-low longitudinal frictional forces during a bobsleigh run is very challenging because of vibrations and much higher forces orthogonal to the driving direction. Therefore we carry out experiments in a controlled environment. This section is based on preliminary studies (mainly the unpublished master thesis ‘Analysis and Simulation of Ice Friction in the Wintersport of Luge’ by J.v. Schleinitz). Previous studies showed that ice friction is dependent on the pressure which is exerted by the gliding body [2]. Therefore, we conduct an experiment in an ice house with a luge sled. The gliding



a) Model generation: Ice house experiments, FEM simulations and track data are combined to a longitudinal and lateral friction model.



b) Driving simulation: The friction model is applied to generate the resulting forces at the runners during the simulation.



c) Driver evaluation: The friction model is applied with inputs from the one-track model to yield the actual and optimal forces at the runners. In combination with the aerodynamic drag force a relative energy loss is determined. Using this definition, the smaller the energy loss the better the driving style is.

Figure 1: Graphical overview of this work.

Table 1: Description of the sub- and superscripts used in this paper.

Subscripts	Description
(x, y, z)	body coordinate system
$(\tilde{x}, \tilde{y}, \tilde{z})$	coordinate system aligned with driving direction
f	at front runner
f0	at front runner, unrotated
r	at rear runner
cog	at center of gravity
ext	external
aero	aerodynamic
ice	ice frictional
ot	one-track model
fm	friction model
kin	kinetic
pot	potential
loss	loss

experiments are carried out on a flat surface, the mass is kept constant and the contact area is changed. Luge steels have a sharp edge at the cross section, while bobsled runners are round. For our experiment, using luge steels has the advantage that a wide range of contact areas and therefore pressures can be studied in this controlled experiment. A finite element simulation is then used to determine the pressure which is exerted on the ice. The resulting correlation between contact pressure and friction can then be applied to bobsled runners by simulating their geometries to determine the contact pressure.

2.2.1. Ice house experiments

Diverse samples are prepared for the investigation of ice friction, with special attention given to the contact pressure. In contrast to most other publications, the pressure is altered by changing the contact area, instead of the normal force. The samples are based on luge steels from the German national team with varying contact area geometries and are named Alpha, Beta, Gamma and Delta. Details are specified in Table 6. The numbers indicate different versions of a luge steel, which are generated by changing the set-up of luge steel and runner.

There are two variations regarding the pressure. The cross section is altered by tilting the luge steel on the runner, which is common practice in luge races. The rocker radius, i.e. the radius of the steels from a lateral point of view, is changed by bending the luge steels and compensating the occurring gap between luge steel and runner. The specific geometries of the samples are confidential but not needed for implementing the methods described in the context of this paper.

The reached initial speed is $8.5 \pm 0.5 \text{ km/h}$. To equalize the effect of a hill slope in the ice house, all test runs are carried out in the opposite direction as well. The frictional force F_x^{ice} is determined for an uphill and a downhill run and then averaged. The experimental conditions are shown in Table 4.

Table 2: Description of the symbols used in this paper.

Symbols	Description
v	velocity
m	mass
E	energy
s	distance
h	height
p	pressure
r	radius
κ	hill slope angle
F_x, F_y, F_z	forces in x, y and z
a_x, a_y, a_z	accelerations in x, y and z
M_x, M_y, M_z	torque in x, y and z
$\varphi, \dot{\varphi}, \ddot{\varphi}$	angle/ angular velocity/ acceleration around the roll axis (x)
$\theta, \dot{\theta}, \ddot{\theta}$	angle/ angular velocity/ acceleration around the pitch axis (y)
$\psi, \dot{\psi}, \ddot{\psi}$	angle/ angular velocity/ acceleration around the yaw axis (z)
J_{yy}, J_{zz}	principal moment of inertia around the y-/ z-axis
δ	steering angle
γ	roll-split angle
α_f, α_r	side slip angles at the runners
β	chassis side slip angle (at cog)
l_F, l_R	distance front/rear axle to cog
$C_x A_x, C_y A_y$	aerodynamic drag area
R, T	air parameters: ideal gas constant, temperature
μ_x, μ_y	friction coefficient in x-/y-direction
C_y, E_y, K_y, ζ_y	friction model parameters in y-direction
$B_x, C_x, D_x, E_x, \zeta_x$	friction model parameters in x-direction
\mathbf{A}	rotation matrix

Table 3: Utilized Sensors and measured parameters

Sensor	Measured parameter
Accelerometer	Accelerations: a_x, a_y, a_z
Gyroscope	Rotational velocities: $\dot{\varphi}, \dot{\theta}, \dot{\psi}$
Optical Speed-over Ground Sensor	Velocity in the xy-plane: v Side slip angle: α
Rotational Potentiometer	Steering angle: δ Roll-split angle: γ

Table 4: Ice house experiment conditions

Ice Temp.	Ambient Temp.	Humidity	Atmospheric Pressure
$-1.5^\circ C$	$2^\circ C$	62%	947hPa

2.2.2. Data processing

The total energy E^{tot} of a gliding sled can be described as the sum of the potential energy E^{pot} , the kinetic energy E^{kin} and the loss energy E^{loss}

$$E^{\text{tot}} = E^{\text{pot}} + E^{\text{kin}} + E^{\text{loss}}, \quad (2)$$

with $E^{\text{loss}} = E^{\text{aero}} + E^{\text{ice}}$.

The loss energy comprises of an aerodynamic part E^{aero} and an ice frictional part E^{ice} . Assuming a distance s , an altitude $h(s)$ and a velocity function $v(s)$, it results for a section from a point s_0 to s_1

$$\begin{aligned} E^{\text{pot}} &= m \cdot g \cdot (h(s_1) - h(s_0)), \\ E^{\text{kin}} &= \frac{1}{2} \cdot m \cdot (v(s_1)^2 - v(s_0)^2), \\ E^{\text{aero}} &= \int_{s_0}^{s_1} F_x^{\text{aero}} ds, \end{aligned} \quad (3)$$

with m being the mass, g the earth's gravitational acceleration and F_x^{aero} the aerodynamic force. It can be calculated with the drag equation by using v and the ambient air conditions

$$F_x^{\text{aero}} = \frac{C_x A_x \cdot v^2 \cdot \rho}{2}, \quad \rho = \frac{p^{\text{air}}}{R \cdot T}, \quad (4)$$

whereby C_x is the drag coefficient, A_x the cross section area, p^{air} the ambient pressure, R the universal gas constant and T the temperature of the air.

For the frictional force F_x^{ice} , it holds

$$F_x^{\text{ice}} = \frac{d E^{\text{ice}}}{ds} = - \frac{d (E^{\text{pot}} + E^{\text{kin}} + E^{\text{aero}})}{ds} \quad (5)$$

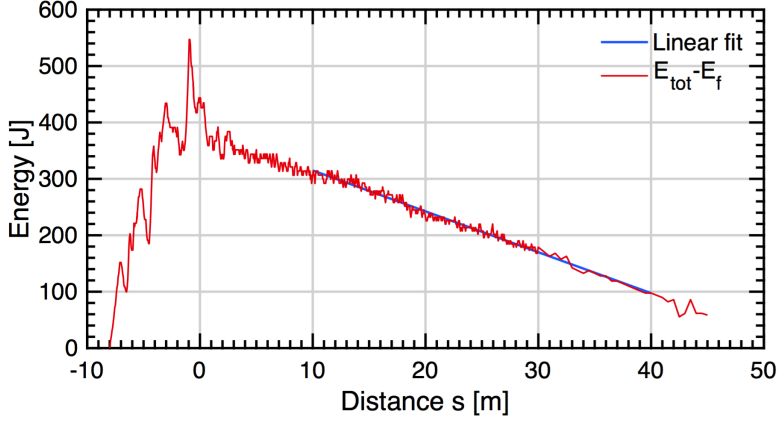


Figure 2: Energy diagram of a one run of the gliding experiment in the ice house. The negative slope represents the frictional force.

by using the law of energy conservation. The friction coefficient μ_x for sliding friction is defined as

$$\mu_x = \frac{|F_x^{\text{ice}}|}{|F_z|} = \frac{|F_x^{\text{ice}}|}{m \cdot g \cdot \cos(\kappa)}, \quad (6)$$

whereby F_z designates the normal force and κ the hill slope angle. A linear least square fit was used to identify the slope of the energy function $\frac{dE}{ds}$ as shown in Figure 2. To minimize unwanted effects from the laying-down or sitting-up of the driver, only the middle section of the gliding phase was utilized.

2.2.3. Finite element simulation

A three-dimensional, linear elastic, static contact finite element (FEM) simulation is used to determine the contact pressure that a luge steel exerts on the ice. The simulation program is based on the MatLab Code ‘Linear Elasticity’ from Alberty et al. [29]. In addition, the contact algorithm from Schröder and Blum [30] is applied which is based on an accelerated projective SOR (Successive Over-Relaxation) approach. Hexahedral elements are introduced, boundary conditions are defined and the post-processing is altered to generate the desired output parameters. Luge specific measurement tools and algorithms are used to generate a three dimensional hull model of a luge steel. Note, that other approaches would yield similar results for the geometry generation, therefore, we do not describe the procedure in detail. Figure 3 shows exemplary results for two samples. The differences in contact pressure and width are clearly visible.

2.2.4. Longitudinal friction equation

The ice house experiment yields the friction coefficients of the samples and the FEM simulation the corresponding contact pressures. We fit a quadratic least square fit to inter- and extrapolate the measured data. A quadratic approach seems to be a natural choice for us, because other works suggested that there exists a minimum of $\mu_x(p)$ [2].

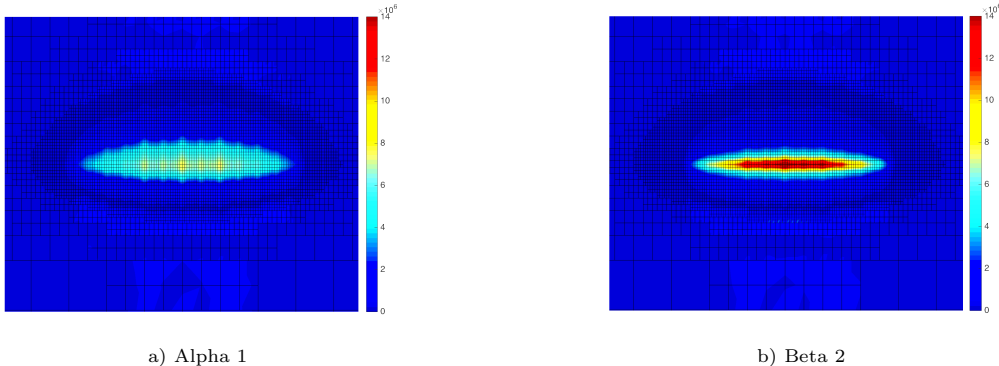


Figure 3: Exemplary ice surface pressure distributions of two samples from the experiment. The sample *Alpha 1* shows the lowest and *Beta 2* the highest maximal pressure.

For the longitudinal direction we propose the following model using the relation between p and μ_x

$$F_x = -\mu_x \cdot F_z \cdot \cos(\alpha), \quad (7)$$

$$\text{with } \mu_x = 10^{-3} \cdot \min\{\zeta_x \cdot (B_x \cdot p^2 - C_x \cdot p + D_x), E_x\}.$$

Thereby, B_x, C_x, D_x are parameters from the quadratic fit. The parameter E_x is an upper threshold for μ_x , which is necessary since the quadratic fit itself would be unconstrained towards very high pressures. The cosine of the side slip angle α is included to have a reasonable transition from longitudinal to lateral friction in the range of $-90^\circ \leq \alpha \leq 90^\circ$. For example, when the bob is sliding purely laterally ($\alpha = \pm 90^\circ$) we expect the longitudinal force to be zero. The parameter ζ_x accounts for asperities. In the ice house and in the FEM simulation, the ice was smooth without asperities. For these circumstances it holds $\zeta_x = 1$. However, on a real track there can be significant asperities, leading to higher contact pressures. This can be accounted for by setting $\zeta_x > 1$.

2.3. Lateral friction model

The accurate modeling of lateral friction is a key element for realistic driving behavior in a driving simulator. The frictional forces are one order of magnitude higher than for the longitudinal direction, resulting in a lateral acceleration which can be measured with good accuracy. Therefore, we can use a more direct approach than for the longitudinal friction and use track data for modeling.

2.3.1. Track experiments

As summarized in Table 5, 44 runs with five different drivers were able to be obtained on the bob track in Königssee (Germany). Figure 4 shows an exemplary overview of a run in the time domain. All signals are measured at the mounting position of the corresponding sensors. We transform the accelerations $\{a_x, a_y, a_z\}$ to the center of gravity

$\{a_{x,\text{cog}}, a_{y,\text{cog}}, a_{z,\text{cog}}\}$ using the rotational velocities, accelerations and distance of the sensor to the center of gravity $\{l_x, l_y, l_z\}$ with the principles of rigid body dynamics

$$\begin{pmatrix} a_{x,\text{cog}} \\ a_{y,\text{cog}} \\ a_{z,\text{cog}} \end{pmatrix} = \begin{pmatrix} a_x \\ a_y \\ a_z \end{pmatrix} - \begin{pmatrix} -\dot{\theta}^2 - \dot{\psi}^2 & \dot{\varphi} \cdot \dot{\theta} - \ddot{\psi} & \dot{\varphi} \cdot \dot{\psi} + \ddot{\theta} \\ \dot{\varphi} \cdot \dot{\theta} + \ddot{\psi} & -\dot{\varphi}^2 - \dot{\psi}^2 & \dot{\theta} \cdot \dot{\psi} - \ddot{\varphi} \\ \dot{\varphi} \cdot \dot{\psi} - \ddot{\theta} & \dot{\theta} \cdot \dot{\psi} + \ddot{\varphi} & -\dot{\varphi}^2 - \dot{\theta}^2 \end{pmatrix} \begin{pmatrix} l_x \\ l_y \\ l_z \end{pmatrix}. \quad (8)$$

Thereby, we assume that the rotation speeds are constant for the whole body, i.e. rigid body dynamics can be applied. This is a simplification, especially for the front part of the bob because of the roll-split.

By geometric considerations, the side slip angle at other points along the x-axis can be calculated using the distance l_s from the sensor to the desired point and the yaw rate. For the side slip angle at the rear axle it holds

$$\alpha_r = \alpha - \frac{\dot{\psi} \cdot l_{s-r}}{v}, \quad (9)$$

with α being the side slip angle measured at the sensor's position. For the front axle, the steering angle δ has to be considered as well

$$\alpha_f = \alpha - \frac{\dot{\psi} \cdot l_{s-f}}{v} + \delta. \quad (10)$$

Table 5: Data set overview for track experiments, the sample rate was downsampled to 100Hz.

Driver	Number of runs	Driver class
A1	9	Top level
A2	12	Top level
A3	7	Top level
B1	12	Advanced
C1	4	Junior
total	44	

2.3.2. One-track model of a bobsled

For modeling lateral friction we need the forces at the runners which are not measured directly. Therefore, we create a one-track model of a bobsled. In a one-track model, the left and right tire on each axis are combined to one tire [31]. Figure 5 depicts the specific one-track model from three different angles.

The model contains a single front and rear runner. The front runner can rotate around its z-axis (δ), while the rear axle is static. In addition to a standard road car model, there is a rotary joint which rotates the front around the roll-split of the bob (γ). At the center of gravity the bob has the velocity v in the direction β . In consideration of the external forces $F_{x,\text{ext}}$ and $F_{y,\text{ext}}$ acting at the center of gravity (e.g. aerodynamic forces or wall contacts), the longitudinal, lateral and angular momentum equalities are

$$m \cdot a_{x,\text{cog}} = F_{x,r} + F_{x,f0} + F_{x,\text{ext}}, \quad (11)$$

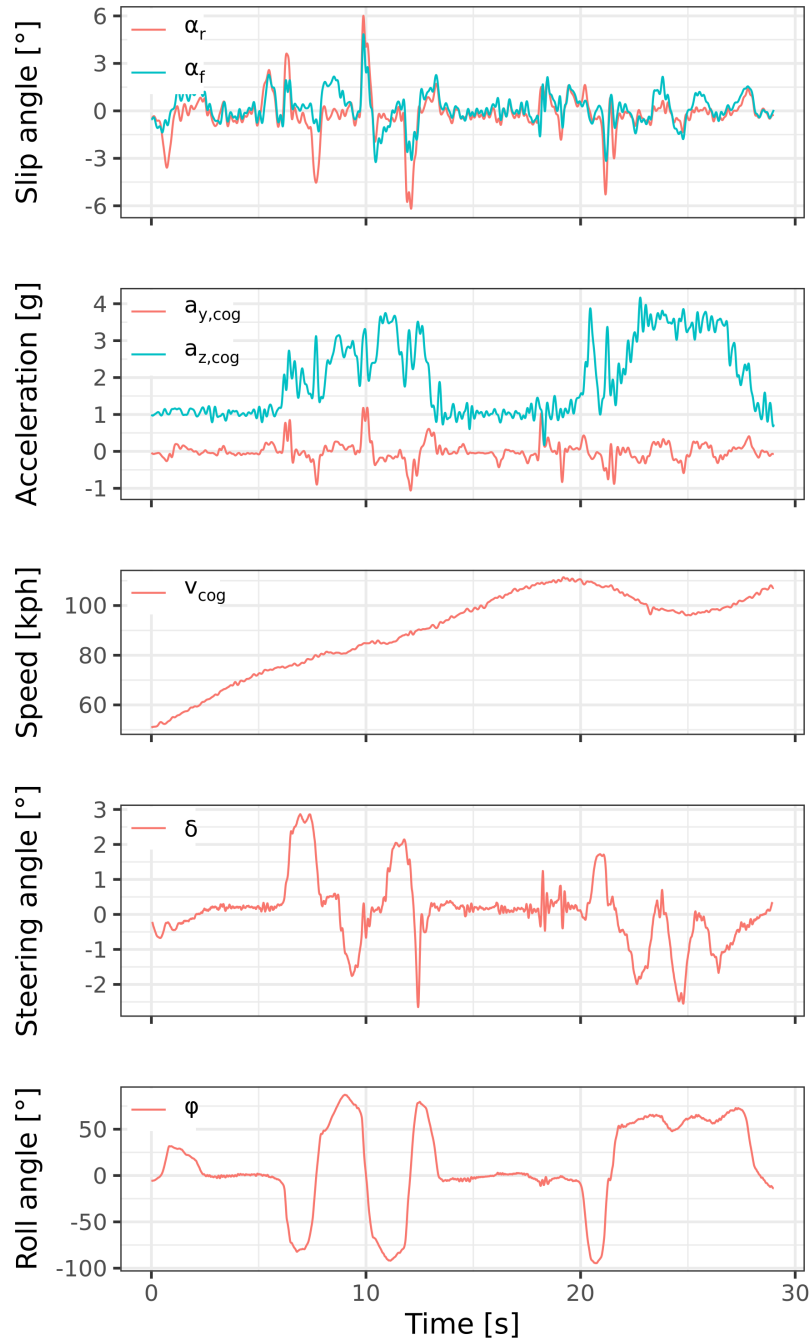


Figure 4: Exemplary overview of selected measurement data in the time domain. The run of an inexperienced driver is shown, which explains why the slip angles on the top panel are relatively high. On the second panel are the accelerations followed by the speed, steering angle and the roll angle. The roll angle is well suited to distinguish the banked corners from each other.

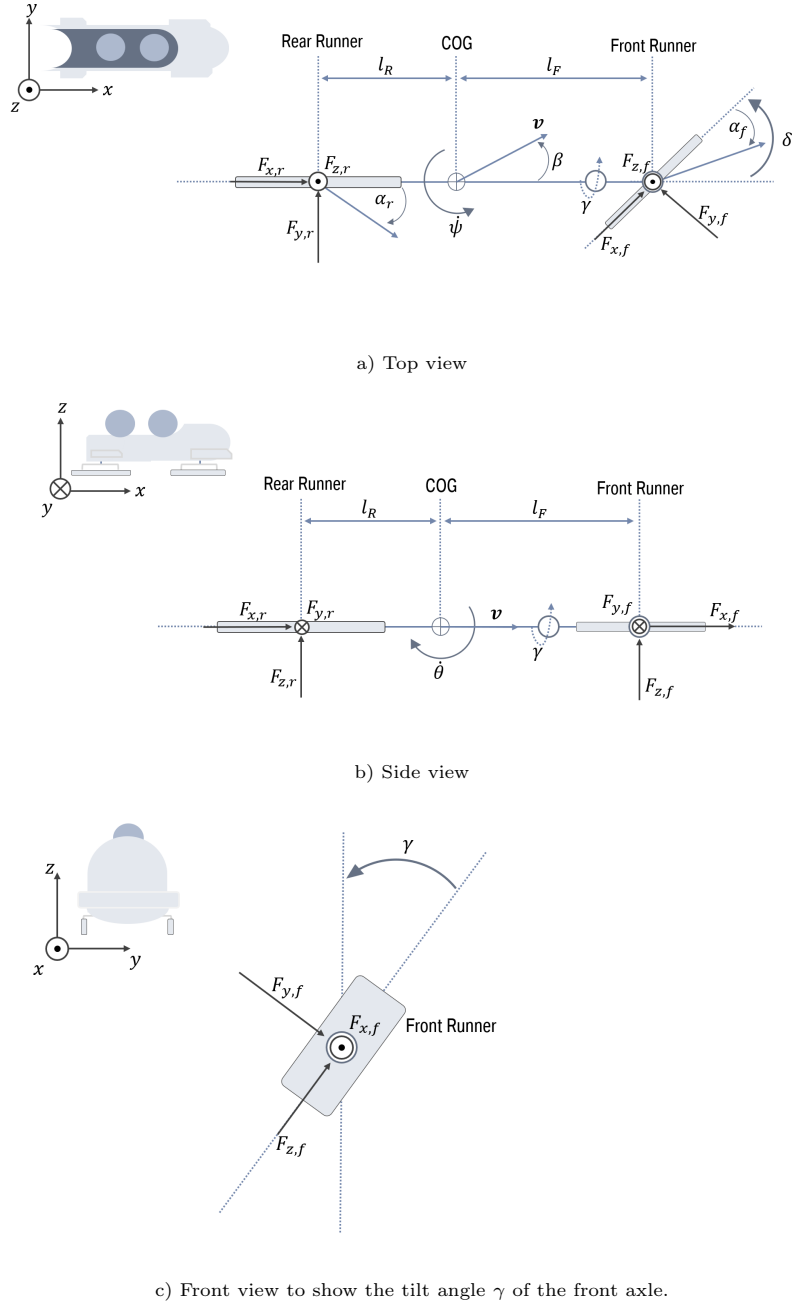


Figure 5: One-track model of a bobsled. The front axle rotates around its z-axis with the steering angle δ , while the rear axle is static. Furthermore, there is a rotational joint to rotate the front around the x-axis by the roll-split angle γ to represent the split of the front and rear part of a bobsled. Thereby, γ includes both the rotation between the bobsled's front and rear part as well as the separate rotation of the front axle.

$$m \cdot a_{y,\text{cog}} = F_{y,r} + F_{y,\text{f0}} + F_{y,\text{ext}}, \quad (12)$$

$$m \cdot a_{z,\text{cog}} = F_{z,r} + F_{z,\text{f0}}, \quad (13)$$

$$J_{zz} \cdot \ddot{\psi} = l_{\text{F}} \cdot F_{y,\text{f0}} - l_{\text{R}} \cdot F_{y,r} + M_{z,\text{f}} + M_{z,r}, \quad (14)$$

$$J_{yy} \cdot \ddot{\theta} = l_{\text{F}} \cdot F_{z,\text{f0}} - l_{\text{R}} \cdot F_{z,r} + M_{y,\text{f}} + M_{y,r}. \quad (15)$$

As an approximation we assume that the torques $M_{y,f}$, $M_{y,r}$, $M_{z,f}$, $M_{z,r}$ are zero. The index ‘f0’ denotes the point at the front axle in the unrotated COG coordinate system, i.e. without the rotations γ and δ . It can be transformed to the front runner coordinate system ‘f’ by first applying the rotation matrix

$$\mathbf{A}_\gamma = \begin{pmatrix} 1 & 0 & 0 \\ 0 & \cos(\gamma) & -\sin(\gamma) \\ 0 & \sin(\gamma) & \cos(\gamma) \end{pmatrix} \quad (16)$$

and afterwards the rotation δ . Since δ is measured in the already rotated coordinate system (the front axle’s steering axis rotates with the roll-split), the rotation axis of δ is dependent on γ leading to the rotation matrix

$$\mathbf{A}_\delta = \begin{pmatrix} \cos(\delta) & -\cos(\gamma)\sin(\delta) & -\sin(\gamma)\sin(\delta) \\ \cos(\gamma)\sin(\delta) & \sin^2(\gamma)\tilde{\delta} + \cos(\delta) & -\sin(\gamma)\cos(\gamma)\tilde{\delta} \\ \sin(\gamma)\sin(\delta) & -\sin(\gamma)\cos(\gamma)\tilde{\delta} & \cos^2(\gamma)\tilde{\delta} + \cos(\delta) \end{pmatrix}, \quad (17)$$

with $\tilde{\delta} = 1 - \cos(\delta)$.

We define the transformation matrix from the ‘f0’ to the ‘f’ coordinate system \mathbf{A} as

$$\mathbf{A} = \mathbf{A}_\delta \mathbf{A}_\gamma. \quad (18)$$

Consequently, it holds

$$\begin{pmatrix} F_{x,\text{f}} \\ F_{y,\text{f}} \\ F_{z,\text{f}} \end{pmatrix} = \mathbf{A} \begin{pmatrix} F_{x,\text{f0}} \\ F_{y,\text{f0}} \\ F_{z,\text{f0}} \end{pmatrix}. \quad (19)$$

and for the inverse transformation

$$\begin{pmatrix} F_{x,\text{f0}} \\ F_{y,\text{f0}} \\ F_{z,\text{f0}} \end{pmatrix} = \mathbf{A}^{-1} \begin{pmatrix} F_{x,\text{f}} \\ F_{y,\text{f}} \\ F_{z,\text{f}} \end{pmatrix} = \mathbf{A}^{\text{T}} \begin{pmatrix} F_{x,\text{f}} \\ F_{y,\text{f}} \\ F_{z,\text{f}} \end{pmatrix}, \quad (20)$$

with $\mathbf{A}^{\text{T}} = \mathbf{A}^{-1}$ since \mathbf{A} is orthogonal.

2.3.3. Limitations

The measured data does not provide enough information for a two-track model, which would contain all four runners. Therefore, the effect of high roll accelerations and the resulting lateral load transfer are not considered. What is more, the acceleration transformation in (8) does not account for the roll split of the bob. During high roll accelerations, the rear and front part of the bob are accelerated to each other. Because of these properties, we exclude data for fitting of the friction model for which the roll acceleration is higher than a certain threshold. We choose a threshold of $100^\circ/s^2$ as a compromise between excluding the problematic high roll accelerations and keeping a sufficient amount of data from cornering phases.

2.3.4. Lateral friction equation

We fit a nonlinear regression model to the data set by adapting a part of the Pacejka ‘Magic Formula Tyre Model’, which is an empiric model for tire road friction [32]. Since the bob glides in longitudinal direction, it is sufficient to model pure lateral friction. We propose the following equation as a lateral friction model

$$F_y = \mu_y \cdot \zeta_y \cdot F_z \cdot \sin \left(C_y \cdot \arctan \left(B_y \cdot \alpha - E_y \cdot \left(B_y \cdot \alpha - \arctan (B_y \cdot \alpha) \right) \right) \right), \quad (21)$$

$$\text{with } B_y = \frac{K_y}{C_y \cdot \mu_y \cdot \zeta_y \cdot F_z}.$$

Thereby, μ_y , ζ_y , C_y , K_y and E_y are regression parameters, α and F_z predictor variables. The parameters are determined with the *MathWorks*[®] *MATLAB* *fitnlm* function which fits a specified nonlinear regression model to given data. We use a subset of the track data set (three days with similar bob settings and track conditions) for fitting the friction model. We predefine E_y to control the trend of F_y towards higher absolute values of α , since the measured range of slip angles was relatively small. We set $E_y = 0.99$ to slightly increase F_y with increasing α . This helps the driving simulation to be stable and predictable for higher slip angles. The parameter ζ_y can be used as a tuning parameter, e.g. to account for asperities similar to the equation for the longitudinal friction.

From the accelerations at the center of gravity, the forces at the front and rear runner need to be calculated to fit a friction model. A problem is that it is not possible to determine the split of $F_{x,\text{cog}}$ into $F_{x,\text{f0}}$ and $F_{x,\text{r}}$ from the measured data with the one-track model. Furthermore, the force $F_{x,\text{cog}}$ is very small compared to the other two forces and sensitive to the alignment of the sensor which leads to a high relative measurement error. $F_{x,\text{r}}$ is not needed to determine a lateral friction model, however, $F_{x,\text{f0}}$ has to be known because of the required rotations γ and δ to yield the forces at the front runner. To solve this problem we pre-define $F_{x,\text{f}}$ in the front runner coordinate system using the already stated equation for longitudinal friction (7). In our case, this shows the need to consider both longitudinal and lateral friction in one model. According to (19) it holds for the x-component of the matrix equation

$$A_{(1,1)} F_{x,\text{f0}} + A_{(1,2)} F_{y,\text{f0}} + A_{(1,3)} F_{z,\text{f0}} = F_{x,\text{f}}. \quad (22)$$

Consequently, $F_{x,\text{f0}}$ is given by

$$F_{x,\text{f0}} = A_{(1,1)}^{-1} \left(F_{x,\text{f}} - A_{(1,2)} F_{y,\text{f0}} - A_{(1,3)} F_{z,\text{f0}} \right). \quad (23)$$

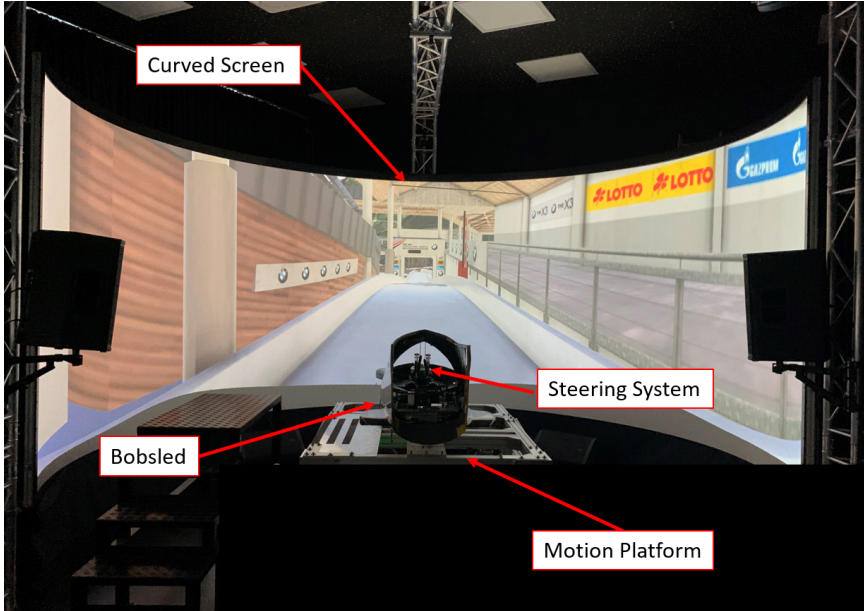


Figure 6: BMW bobsled driving simulator setup.

With that, the necessary information is given to calculate all desired forces.

2.4. Application in driving simulation

The friction model here presented is deployed at the BMW bobsled simulator, which is serving as a training ground for the German national bobsleigh team in preparation for the 2022 Olympic Winter games. Its hardware is based on the BMW Motorsport simulator and is located in Munich [24, 26]. Figure 6 shows the bob simulator setup.

The mechanical assembly consists of a 210° curved screen which surrounds a four degree-of-freedom motion platform on which an original bobsled is attached. The yaw rate $\dot{\psi}$, pitch rate $\dot{\theta}$ and roll rate $\dot{\varphi}$ as well as heave motion (translation along the z-axis) can be rendered. The platform motion is controlled by a custom motion cueing algorithm. In addition, the steering mechanism of the bobsled is altered and includes a force feedback system.

The friction model is needed in the bob simulator to calculate the resulting forces at the runners based on inputs from the simulation such as for example the normal forces and the slip angles at the runners. We use the equations (7) and (21) for the longitudinal and lateral frictional forces, respectively.

A precise modeling of the longitudinal friction force is required to achieve realistic run times and velocities on the track in the simulator. However, the pressure p cannot be simulated by FEM as described in Section 2.2 since the model needs to be realtime executable. Therefore, we propose a lookup for the pressure p as a function of F_z and the track radius around the y-axis of the bob $r_{y,\text{track}}$, which can be calculated by using the pitch rate and velocity

$$r_{y,\text{track}} = -\frac{v}{\dot{\theta}}. \quad (24)$$

The lookup has to be generated for the front and rear runner, due to different geometries. As for luge steels, the cross section and rocker radius influence the pressure. We note that the geometries of bob runners provided by the German national team are confidential. Therefore the results of the finite element simulations and the described lookup for the bob runners are not published.

The forces generated by lateral friction have a strong impact on vehicle dynamics and are as a result decisive for a realistic driving behavior of the simulator. Therefore, the friction model is subject to continuous development based on data analysis and driver feedback. The data driven approach of this work aims to be a good starting point for further development. In the first tests, the driving behavior was described to be realistic by professional athletes (World and Olympic champions in bobsleigh). However, the detailed analysis and validation of a driving simulator is an extensive task and will not be part of this paper.

2.5. Application in Driver evaluation

In bobsleigh, the achieved runtime on a track is decisive for winning races. Unsurprisingly, it has been the main criteria to evaluate bobsleigh drivers to this day. However, the runtime is influenced by many factors:

- Start speed
- Track conditions
- Ambient conditions
- Bobsled performance
- Driver performance

Also, it is track specific and due to its strong sensitivity on outer conditions usually also session specific. Especially when comparing top drivers' performances, it is necessary to have stable track and weather conditions and even then time comparisons are only viable when all runs are carried out within a short time frame. Long-term and trend analysis to capture driver development are therefore hardly possible, if at all.

In contrast, we propose a method to evaluate driver performance on the basis of the developed friction models for longitudinal (7) and lateral friction (21) which can be applied to a data set containing multiple sessions, changing conditions and even different tracks. As stated above, the task of a bob driver is to achieve the fastest runtime. This can be accomplished by minimizing the ratio of traveled distance (from start to finish) and average velocity. Since the track in combination with the bobsled's driving dynamics restrict the possible racing line tightly, we focus on maximizing the average velocity in this work. This seems to be a sufficient approximation since no major deviations in the driven distance could be observed in the available data set. As stated in (2) the only force accelerating a bobsled after the starting phase is the gravitational force. The driver can maximize the positive acceleration, and thereby the velocity, by minimizing the frictional losses which comprise of ice friction and aerodynamic drag.

2.5.1. Aerodynamics

We want to model the aerodynamic drag force dependent on the bobsled's chassis side slip angle β . An increase of the aerodynamic losses with increasing absolute β is expected due to an increased drag area $C_{\tilde{x}}A_{\tilde{x}}$ in the driving direction \tilde{x} . Thereby, we use β to introduce the coordinate system $(\tilde{x}, \tilde{y}, \tilde{z})$ where \tilde{x} is aligned with the driving direction

$$\begin{pmatrix} \tilde{x} \\ \tilde{y} \\ \tilde{z} \end{pmatrix} = \begin{pmatrix} \cos(\beta) & -\sin(\beta) & 0 \\ \sin(\beta) & \cos(\beta) & 0 \\ 0 & 0 & 1 \end{pmatrix} \begin{pmatrix} x \\ y \\ z \end{pmatrix}. \quad (25)$$

We do not have wind tunnel measurements for different side slip angles available, therefore we approximate the so-called yaw sensitivity using simulations from Bello-Millán et al. [33] who provided a diagram of the drag area $C_{\tilde{x}}A_{\tilde{x}}$ over yaw angles for an 'Ahmed body'. An Ahmed body depicts a simplified vehicle geometry which is usually used for simulation studies of automobiles. However, its shape is also comparable to a bobsled, it has a rounded front section and a straight lateral surface. The similarities should be sufficient to yield a yaw sensitivity in the same order of magnitude. From a diagram in the work of Bello-Millán et al. [33] we extracted an increase of the drag area $\Delta_{C_{\tilde{x}}A_{\tilde{x}}}$ over yaw angle in the range from $0 - 10^\circ$

$$\begin{aligned} \Delta_{C_{\tilde{x}}A_{\tilde{x}}}^{\text{Ahmed}} &= 3.2 \text{ \%}/^\circ, \\ \text{with } \frac{A_y}{A_x} &\approx 2.3. \end{aligned} \quad (26)$$

For a bobsled we determined

$$\frac{A_y}{A_x} \approx 5 \quad (27)$$

which is 2.17 times the surface ratio in (26). As a rough approximation we assume the relative increase to scale linearly with the relative surface area differences

$$\Delta_{C_{\tilde{x}}A_{\tilde{x}}} \approx 2.17 \cdot \Delta_{C_{\tilde{x}}A_{\tilde{x}}}^{\text{Ahmed}} \approx 6.94 \text{ \%}/^\circ. \quad (28)$$

This leads to a dependency of the drag area on β

$$C_{\tilde{x}}A_{\tilde{x}} = C_xA_x + 0.0694 \cdot C_xA_x \cdot |\beta| \quad (29)$$

for a bobsled. The resulting aerodynamic force in driving direction $F_{\tilde{x}}^{\text{aero}}$ is then determined with (4).

It has to be noted that this is an approximation yielding only the order of magnitude of the effect. Wind tunnel experiments to determine the exact values should be conducted. What is more, the effect of track walls and the rotation rates of the bobsled are not considered in this approximation. Also the aerodynamic influence of the roll-split of the bob, which was examined by Sciacchitano and Pattnaik [34] is not considered. To improve the aerodynamic model, computational fluid dynamics simulations should be conducted which include the stated parameters.

2.5.2. Driver evaluation criteria

We assume that the optimal state, i.e. the state with minimal frictional losses, occurs when the bob is traveling in a straight line with no side slip angle at the runners or the center of gravity. For ice friction, this follows directly from our proposed friction models, since the lateral friction is much higher than the longitudinal friction. A similar effect is found for aerodynamics in Section 2.5.1. The consequence is that drifts should be avoided so as not to increase ice friction at both axles. Furthermore, the bobsled's chassis side slip angle β should be zero to be aerodynamically optimal.

Apart from this qualitative statement, we can calculate the effect of drifts for a quantitative analysis using the forces which act against the driving direction. Using the friction and aerodynamic models, the force acting against the driving direction $F_{\bar{x}}$ can be determined using the coordinate transformation in (25). It is compared to the force in x-direction in the body coordinate system F_x , which we consider to be optimal. Of course, this optimum cannot be reached on a real track where steering and lateral forces are necessary, however, it is suited as a basis for comparison. We calculate $F_{\bar{x}}$ and F_x for the front runner, rear runner and for the aerodynamic drag using the coordinate transformation in (25). As an evaluation criteria for the driving style we integrate these forces, which leads to energies and compare the actual and minimal energy loss. First, we calculate the optimum, i.e. a theoretical, minimal loss energy in x-direction

$$E_{\text{loss}}^{\text{tot}} = \int_{s_0}^{s_1} F_{x,f} + F_{x,r} + F_x^{\text{aero}} ds, \quad (30)$$

whereby s_0 and s_1 depict the start and finish at the track. Next, we propose several metrics based on relative loss energy increases

$$\begin{aligned} \Delta E_{\text{loss},f}^{\text{ice}} &= \frac{\int_{s_0}^{s_1} F_{\bar{x},f0} - F_{x,f} ds}{E_{\text{loss}}^{\text{tot}}}, \\ \Delta E_{\text{loss},r}^{\text{ice}} &= \frac{\int_{s_0}^{s_1} F_{\bar{x},r} - F_{x,r} ds}{E_{\text{loss}}^{\text{tot}}}, \\ \Delta E_{\text{loss}}^{\text{aero}} &= \frac{\int_{s_0}^{s_1} F_{\bar{x}}^{\text{aero}} - F_x^{\text{aero}} ds}{E_{\text{loss}}^{\text{tot}}}, \\ \Delta E_{\text{loss}}^{\text{tot}} &= \Delta E_{\text{loss},f}^{\text{ice}} + \Delta E_{\text{loss},r}^{\text{ice}} + \Delta E_{\text{loss}}^{\text{aero}}. \end{aligned} \quad (31)$$

We use the term $F_{\bar{x},f0} - F_{x,f}$ for the front to accommodate for the losses which arise by rotating the front runner with the angles γ and δ . The reason why we analyze the losses relative to the optimum is that the absolute energy difference is influenced by the velocity and normal forces and thus dependent on track conditions.

In summary, $\Delta E_{\text{loss}}^{\text{tot}}$ can be interpreted as an overall score for driver evaluation. The smaller the relative energy increase to the optimum, the better the driver. By analyzing the steering and side slip angles and comparing the losses arising at the front and rear axle we can distinguish and evaluate different driving styles. Note that a lower energy loss does not necessarily imply a faster runtime when comparing different runs. Energy lost at the beginning of a track has a greater influence on the runtime than the same amount of energy lost near the finish. If needed the runtime influence can be calculated from the energy losses and corresponding positions on the track. In the case of driver

evaluation we assume the energy difference to be more meaningful than the runtime difference as it is applicable to different tracks and conditions.

Apart from drivers, this method can also be used to evaluate the characteristic of different bob tracks. For track specific bobsleigh adjustment it might be interesting to compare how much energy is lost on the front axle compared to the rear axle.

2.5.3. Limitations

In principle this driving style evaluation should be independent of the conditions on the track. In contrast, the classic metrics such as top speed or runtime strongly depend on the conditions, e.g. Jansons et al. [35] showed that weather conditions had a significant effect on the runtime even on a short starting track. However, also for our proposed relative loss energy difference, there can be indirect influences from the conditions, e.g. there may be circumstances (e.g. very low or high temperatures and a very hard or soft ice surface) for which it is harder to control the bob leading to higher energy losses. Though, for the ice conditions commonly present in training and competitions this effect should be small.

3. Results

3.1. Longitudinal friction model

The results of the ice house experiments and the equivalent FEM simulations are presented in Table 6. Figure 7 shows a graphical overview of friction coefficient and pressure for the samples and the fit for μ_x described in (7). The friction coefficient continuously decreases from Alpha 1 to Gamma 2, where the minimum point is located. Friction rises from that point to Beta 1 and Beta 2. Since the Alpha samples exert little pressure, a decrease of the contact area by reducing the rocker radius from Alpha 1 to Alpha 2 leads to lower friction. Gamma 1 also belongs to the low pressure regime as a pressure decrease to Gamma 3 raises friction and a pressure increase to Gamma 2 reduces friction. In contrast, increasing the pressure from Beta 1 to Beta 2 leads to higher friction. Therefore, the Beta samples are allocated to the high pressure regime. In summary, the resulting parameters for the longitudinal friction model in (7) are listed in Table 7.

Table 6: Experimental and simulation results for ice house experiments with luge steels.

Specimen	Rocker Radius	Cross-Section	$\mu_x [10^{-3}]$	$p_{max} [MPa]$
Alpha 1	high	round, wide	4.5 ± 0.4	7.7 ± 0.4
Alpha 2	low	round, wide	3.8 ± 0.4	8.6 ± 0.5
Beta 1	high	sharp, narrow	4.2 ± 0.4	13.6 ± 0.7
Beta 2	low	sharp, narrow	4.6 ± 0.4	16.0 ± 0.9
Gamma 1	high	normal, narrow	3.0 ± 0.3	10.9 ± 0.6
Gamma 2	low	normal, narrow	2.7 ± 0.3	11.8 ± 0.6
Gamma 3	high	normal, wide	3.3 ± 0.3	9.6 ± 0.5

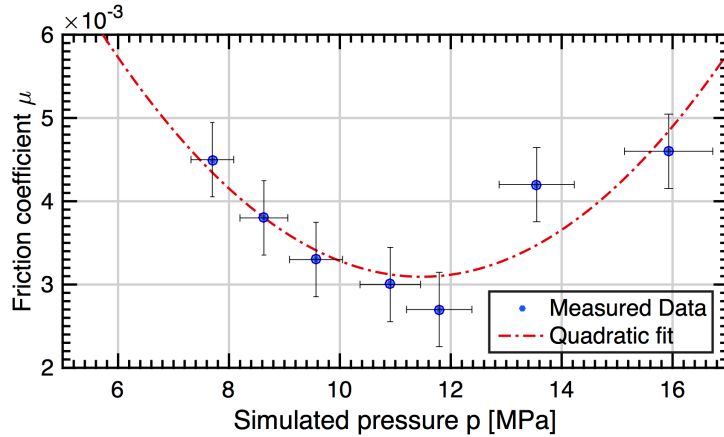


Figure 7: Pressure dependency of the longitudinal friction coefficient μ_x for the ice house experiment specimens with luge steels.

Table 7: Parameters for the longitudinal friction equation (7)

B_x	C_x	D_x	E_x	ζ_x
0.088	2.01	14.66	0.007	1

As stated above, the results of the longitudinal friction coefficient for the bobsleigh runners, i.e. the simulated pressures of the bobsleigh runners cannot be published since the runner geometries are confidential. Therefore, we define μ_x as a fixed value to make the following results of this paper easier to reproduce and not dependent on an undisclosed parameter

$$\mu_x := 0.004. \quad (32)$$

This value lies in the range of our simulated data and is in good agreement with the real life experiments from Poirier et al. [8] and Irbe et al. [10].

3.2. Lateral friction model

Figure 8 and Figure 9 show the measured lateral force F_y over the slip angle α as well as the fitted models for different ranges of F_z . The data (see Table 5) is filtered in the time domain with a low-pass filter and a cutoff frequency of $20Hz$ to reduce noise. The spread of the data points is still high and the correlation with the fits is relatively small for lower F_z . For higher F_z , there is a clearer correlation. In Figure 8b, there seems to be a maximum of $F_{y,f}$ at $\alpha \approx 1^\circ$. A model with more regression parameters could fit this trend better, however, due to the high level of noise we deliberately choose a model that underfits the data slightly.

The rear runner has a distinctly higher cornering stiffness, i.e. it produces more lateral force at a given slip angle than the front runner. The range of the measured data is even smaller, since bob drivers avoid too high slip angles at the rear axle due to dynamic stability (high drifts at the rear lead quickly to uncontrolled oversteer). In summary, the obtained parameters for the lateral friction models are listed in Table 8.

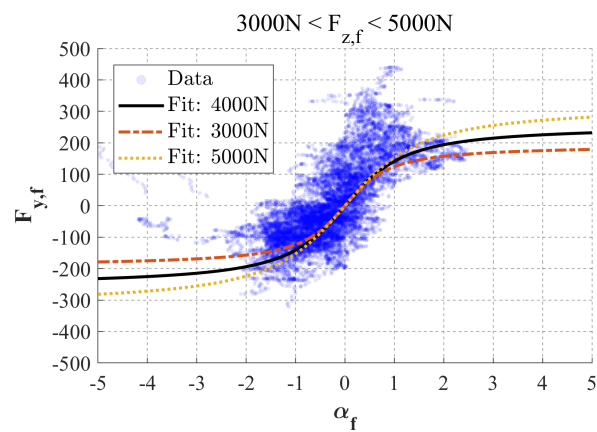
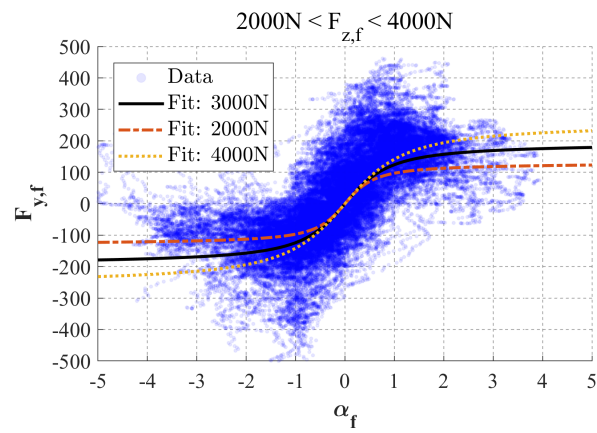
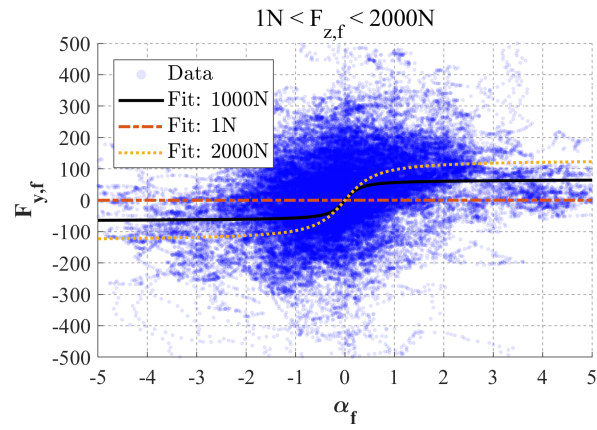


Figure 8: Lateral friction model for the front runner and measured data for different ranges of F_z .

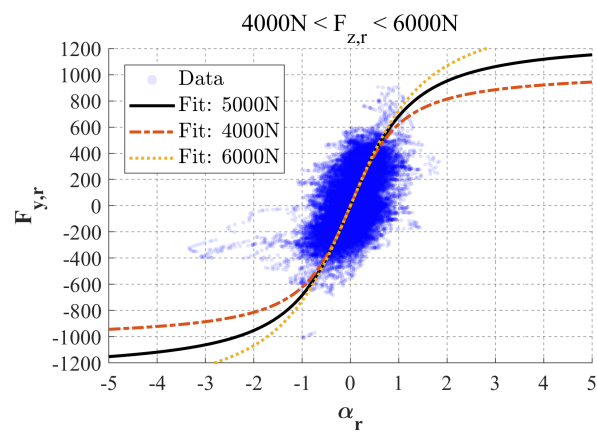
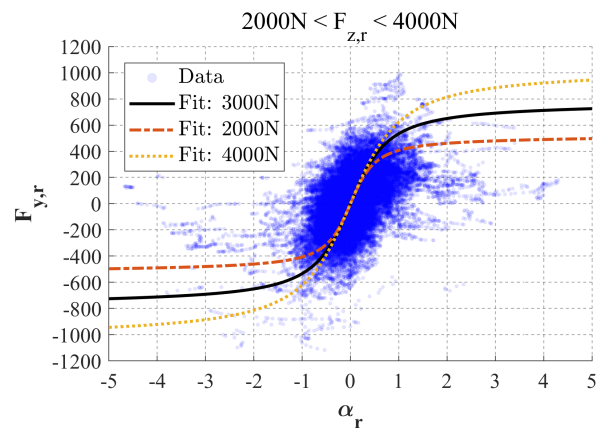
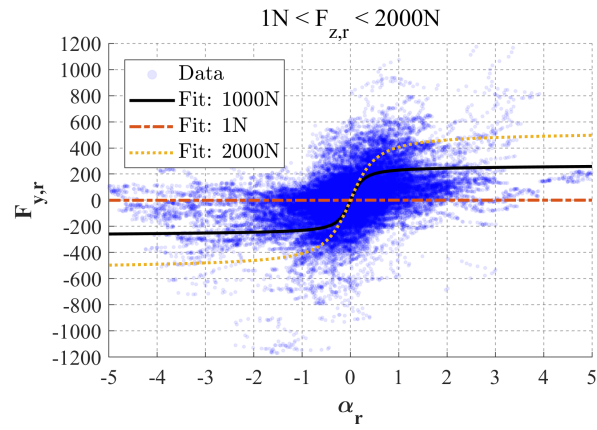


Figure 9: Lateral friction model for the rear runner and measured data for different ranges of F_z .

Table 8: Lateral friction model parameters for front and rear runner. E_y was predefined to the stated value.

Runner	$\mu_y \cdot \zeta_y$	C_y	E_y	K_y
front	2.577	0.024	0.99	10522
rear	3.288	0.076	0.99	49776

3.2.1. Validation

To validate the lateral friction model and to check how general the model is, we compare the lateral force at the center of gravity of the one-track model with the index ‘ot’ $F_{y,\text{cog}}^{\text{ot}}$ with the force $F_{y,\text{cog}}^{\text{fm}}$ yielded by the friction model with the index ‘fm’. Using (8), the force of the one-track model comes directly from measurement. For the friction model, the whole calculation chain is necessary, i.e. determining $F_{z,\text{f}}$, $F_{z,\text{r}}$, α_{f} and α_{r} , applying the friction model with the specified parameters, transforming the determined forces at the front runner and finally summing up the forces at the front and rear runner. Figure 10 shows the root mean square error (RMSE) between the signals. The data used for validation was not used for fitting the model. We compare two different bob tracks, Königssee (KOE) and La Plagne (LAP), from which no data was used for model fitting. Interestingly, the RMSE in La Plagne is even lower than in Königssee. A contribution to the higher error of Königssee can be seen in the time domain in Figure 11. The blue arrows indicate areas where the bobsled hit the wall, which resulted in an external force which is not caused by runner-ice friction and therefore not covered by the friction model. In Königssee, hitting the wall is indeed the correct racing line, especially for the long straight around 500m. In the so-called ‘Labyrinth’ of the track, wall contact is also common (arrow at around 800m). In La Plagne, wall contact is limited to rare driving errors, which is an explanation for the lower RMSE. To sum up, the friction model seems to work well on unseen data and also on a completely different track. Apart from the model developed in this work, the RMSE of the proposed model from Braghin et al. [19] in (1) is shown. The error is considerably higher on both tracks. We opted to compare the models with the provided parameters. Fitting their model to our data, especially if front and rear axle were to be fitted separately, would certainly improve the accuracy.

3.3. Application: Driver evaluation

We compare five drivers on the track in Königssee using the data set described in Table 5. The drivers are divided into the three classes A, B and C according to their level of experience. There are three top level drivers in the A class (the highest level of experience), one advanced driver in the B class (second highest level of experience) and one junior driver in the C class (lowest experience).

At first we analyze the side slip angles and the steering angles between the drivers. Figure 12a depicts the distributions of these variables in the form of boxplots. Since the values are small most of the time, the amount of rarer higher angles cannot be seen. Therefore, Figure 12b shows the ratio of high absolute angles, i.e. over 2° and 4° , respectively.

Looking at the steering angle δ , Driver C1 steers distinctly less than all the other drivers, which holds also for high angle steering. There is not a single instance where C1 steered more than 4° . The low steering angles do not result in low slip angles at the front α_{f} and

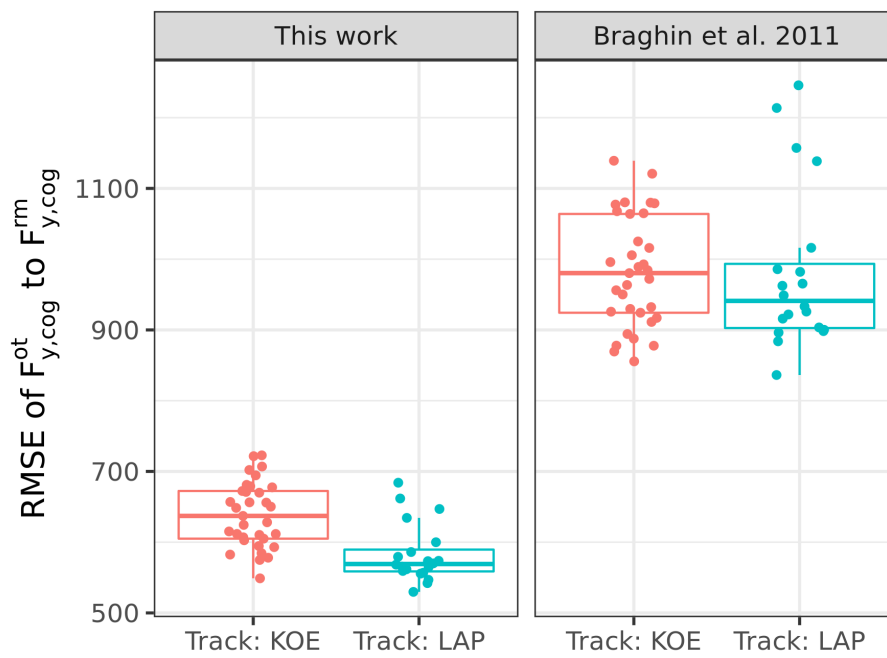


Figure 10: RMSE comparison between the lateral force determined from measurement and the one track model $F_{y,cog}^{ot}$ and the calculated force from the runner model $F_{y,cog}^{rm}$ on two different tracks. Each point accounts for a complete run. The model proposed by Braghin et al. [19] is shown for comparison.

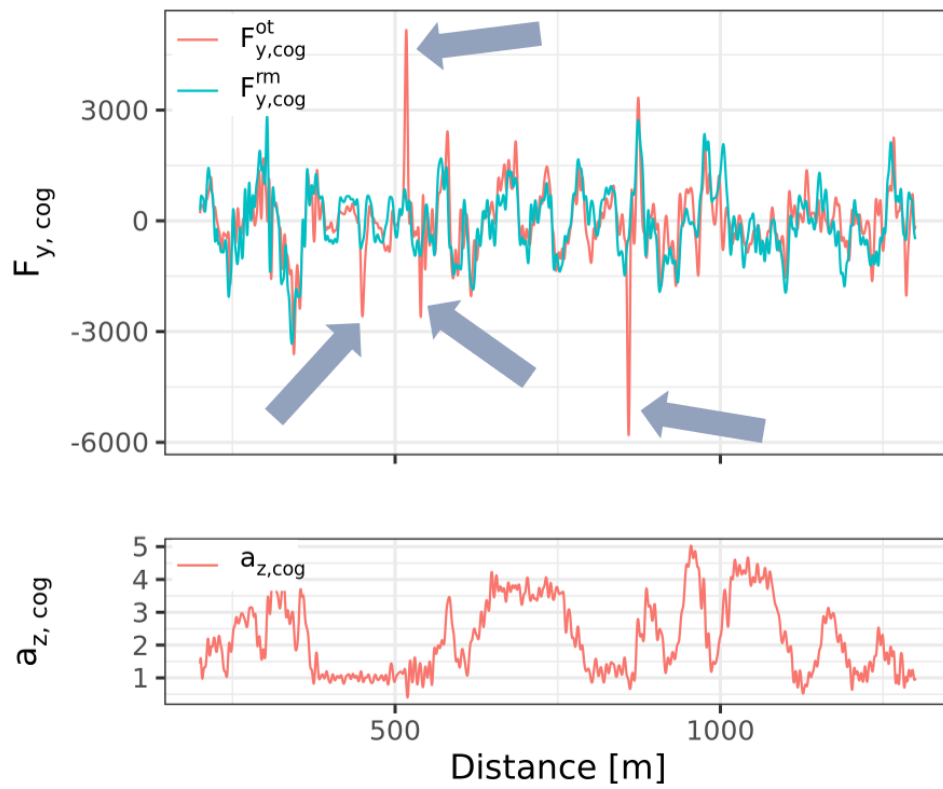
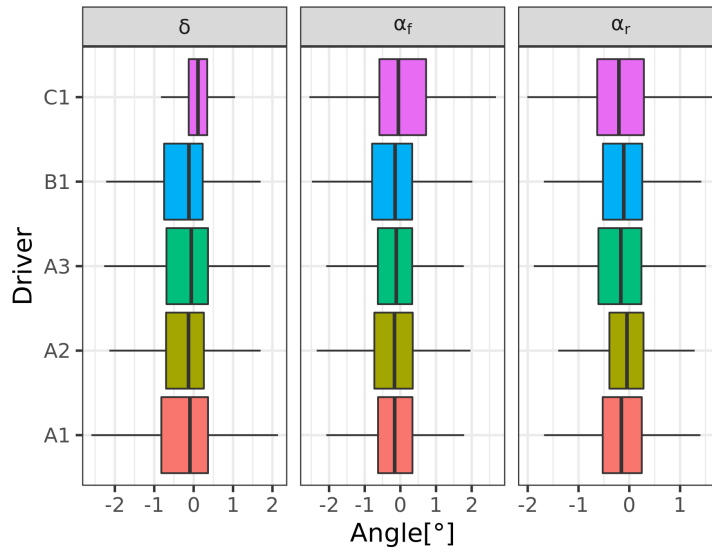
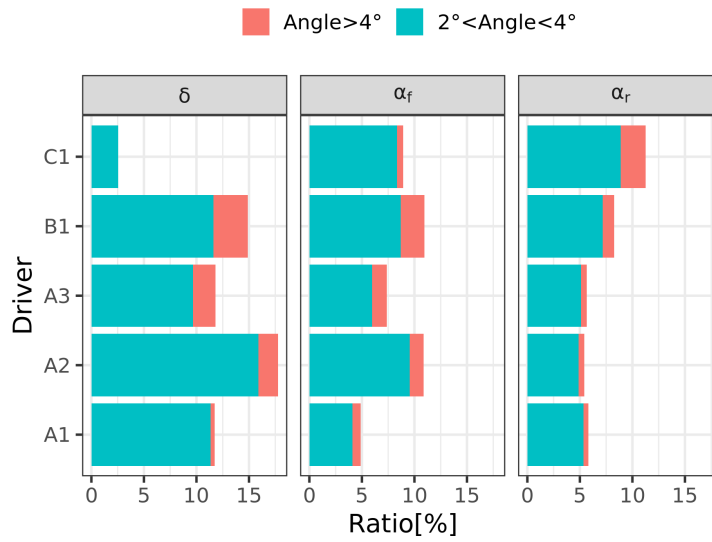


Figure 11: $F_{y,cog}^{ot}$ and $F_{y,cog}^{fm}$ for the track in Königssee. The arrows indicate places where the bobsled hit a wall.



a) Steering and side slip angle overview



b) Overview of high steering and side slip angles.

Figure 12: Driver comparison using measured signals. Clearly, Driver C1 steers much less than all other drivers.

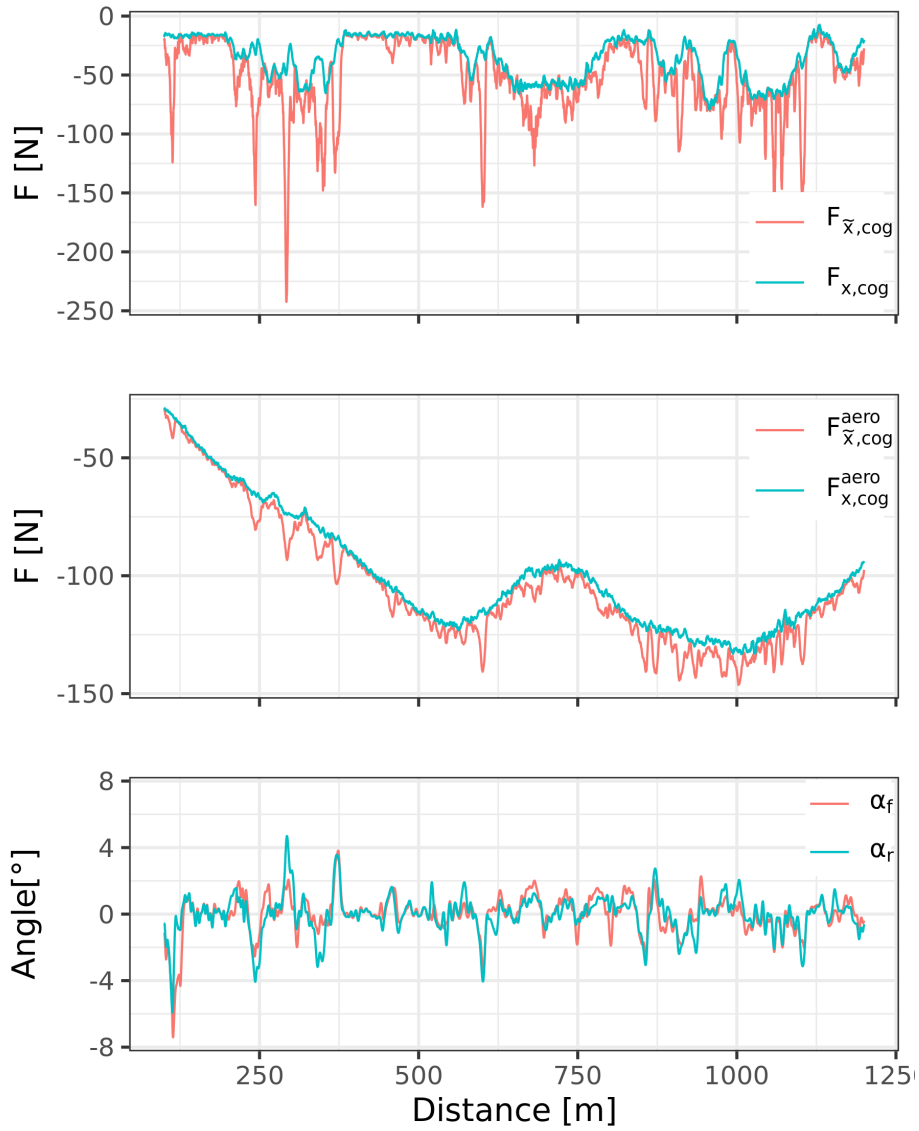
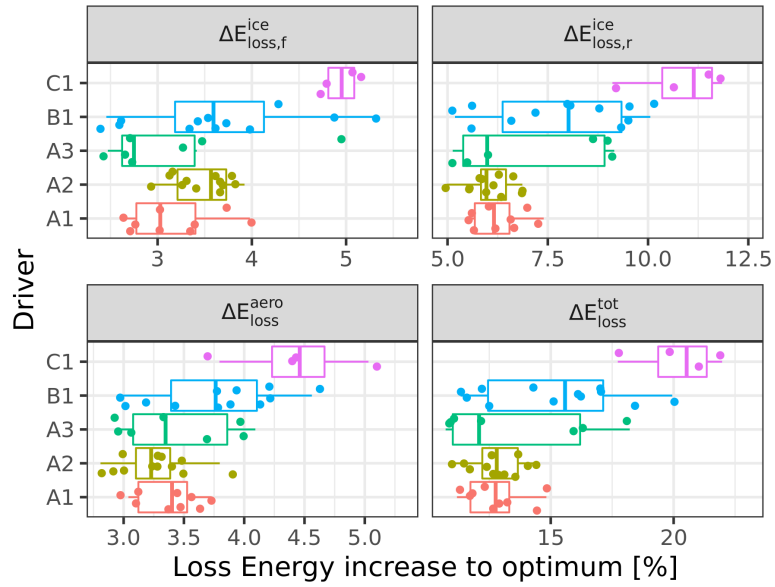
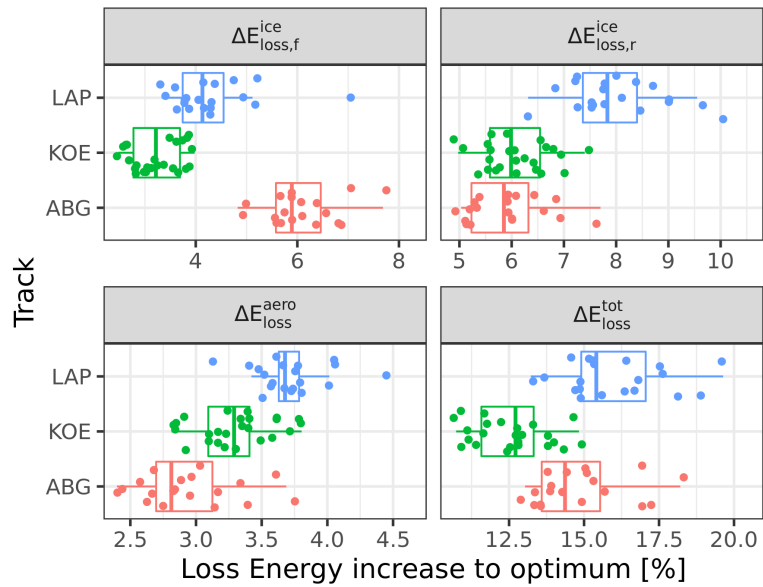


Figure 13: Exemplary overview in the time domain of the forces acting against the direction of movement $F_{\bar{x},cog}$ compared to the force in x-direction in the body coordinate system $F_{x,cog}$ which is considered to be a theoretical optimum. As a reference, the side slip angles are shown as well.



a) Driver comparison on the track Königssee (KOE)



b) Track comparison using only data from the top drivers (A1, A2, A3).

Figure 14: Energy comparisons for the different drivers and tracks. The relative increase of the loss energy with the ideal case as a basis is shown. It can be seen how much energy is lost at the front axle, rear axle, aerodynamically and overall. Every data point accounts for a complete run.

the slip angles at the rear α_r are the highest of all drivers. Comparing the A-Drivers, A2 has the highest percentage of steering angles over 2° and 4° followed by A3 and A1. The slip angles at the front axle produce the same results. On the rear axle the differences are smaller, but here A1 has the lowest amount of high slip angles followed by A1 and A3. The drivers know from experience that drifts at the rear axle cause higher energy loss than at the front axle due to its shape (bigger length and different cross section), which is supported by our runner models (Section 2.3.4): The generated forces are distinctly higher than at the front axle for given slip angles. However, by analyzing only the slip angles it cannot be determined which driving style is more advantageous.

To solve this task we utilize the validated friction model to determine the forces which act against the driving direction and calculate the relative loss energy increase as described in Section 2.5. Figure 13 depicts an exemplary overview of the actual and ideal forces at the center of gravity. It is visible how the side slip angles at front and rear axle lead to higher loss forces. Figure 14 shows the resulting distribution of loss energy increase for each driver and also for different tracks.

3.3.1. Discussion of driving styles

According to Figure 14a, the A drivers have the lowest total losses, followed by B1 and C1 when looking at the medians. This result is in close agreement with the defined classes. Driver C1 is the worst in all categories, therefore it is apparent that the driving style is disadvantageous and the low steering magnitude probably not deliberately chosen but a sign of uncertainty, as one would expect to see with less experienced drivers. Drivers A3 and B1 have a larger spread of values, indicating a more inconsistent driving style. Both have very good and bad runs. The different driving styles of driver A1 and A2 are interesting. We observe that A2 has distinctly higher losses at the front axle due to more steering but slightly less losses on the rear axle and due to aerodynamics. Overall, both approaches result in very similar overall losses. Consequently, in this case both driving styles are equally competitive. We suggest comparing these driving styles on different tracks in a future experiment. For a more detailed analysis, all the signals could be compared in the time or distance domain to give the drivers clear instructions on how to achieve a different driving style if wanted.

3.3.2. Track comparison

As a side result from this work, Figure 14b depicts the resulting energy differences between the tracks in La Plagne (LAP), Königssee (KOE), and Altenberg (ABG). For Altenberg and La Plagne only data from one top driver was available, for Königssee we used the data of the three A-drivers. Interestingly, the overall loss energy pieces together quite differently. Altenberg has distinctly higher losses at the front and less at the rear and aerodynamically. In comparison La Plagne has fewer losses at the front and more at rear. Königssee has overall the lowest losses. In summary, the tracks differ significantly from each other. We think that this information can help to improve the specific bobsled setup for these tracks.

4. Conclusion

This work presents a data driven method to model the relevant aspects of ice friction for vehicle dynamics of a bobsled. The method is not specific to the sport of bobsleigh and can be transferred to other related areas. It shows that the developed friction model is suited for the usage in a driving simulator and capable of distinguishing the driving style differences of top drivers, which is a valuable asset for bobsleigh driver training. Since the driver evaluation depends only indirectly on outer circumstances, long-term driver performance analysis over several seasons could be conducted, which to the best of our knowledge has not been possible up to now . For future research we propose experiments to improve the lateral friction model for lower normal forces. For example ice house experiments where steering maneuvers with a bobsled (e.g. step steer) are conducted can deliver cleaner data than track experiments because of a distinctly lower amount of vibrations on the flat ice house surface. Furthermore, it should be investigated how other factors influence bobsled driving dynamics, for example the gliding velocity or ice surface properties such as temperature, roughness and hardness.

Acknowledgments

We thank the Bob- und Schlittenverband für Deutschland e.V. and its athletes for providing the bobsleigh equipment and conducting all test drives. Furthermore, we want to acknowledge ixent GmbH for fruitful discussions and providing bobsled parameters. We also thank FES (Institut für Forschung und Entwicklung von Sportgeräten) for providing additional measurement data. Special thanks go to Sarah Lederer for proofreading the article. This work was generously supported by BMW AG.

References

- [1] A. M. Kietzig, S. G. Hatzikiriakos, P. Englezos, Ice friction: The effect of thermal conductivity, *Journal of Glaciology* 56 (2010) 473–479. URL: <http://www.ingentaconnect.com/content/igsoc/jog/2010/00000056/00000197/art00009>.
- [2] C. Hainzlmaier, A tribologically optimized bobsleigh runner, Doctoral thesis, TU München, 2005.
- [3] M. Scherge, R. Böttcher, M. Richter, U. Gurgel, High-speed ice friction experiments under lab conditions: On the influence of speed and normal force, *ISRN Tribology* 2013 (2013) 1–6. doi:10.5402/2013/703202.
- [4] M. Scherge, R. Böttcher, A. Spagni, D. Marchetto, High-speed measurements of steel–ice friction: Experiment vs. calculation, *Lubricants* 6 (2018) 26. doi:10.3390/lubricants6010026.
- [5] L. Makkonen, M. Tikanmäki, Modeling the friction of ice, *Cold Regions Science and Technology* 102 (2014) 84–93. doi:10.1016/j.coldregions.2014.03.002.
- [6] M. Hasler, K. Schindelwig, B. Mayr, C. Knoflach, S. Rohm, J. van Putten, W. Nachbauer, A novel ski and snow tribometer and its precision, *Tribology Letters* 63 (2016). URL: <http://link.springer.com/10.1007/s11249-016-0719-2>. doi:10.1007/s11249-016-0719-2.
- [7] J. J. de Koning, G. Degroot, G. J. V. Schenau, Ice friction during speed skating, *Journal of Biomechanics* 25 (1992) 565–571. URL: <GotoISI>://W0S:A1992HZ03200001. doi:10.1016/0021-9290(92)90099-m.
- [8] L. Poirier, E. P. Lozowski, S. Maw, D. J. Stefanyshyn, R. I. Thompson, Experimental analysis of ice friction in the sport of bobsleigh, *Sports Engineering* 14 (2011) 67–72. doi:10.1007/s12283-011-0077-0.
- [9] L. Poirier, Ice Friction in the Sport of Bobsleigh, Canadian theses = Thèses canadiennes, Library and Archives Canada = Bibliothèque et Archives Canada, Ottawa, 2012.
- [10] M. Irbe, K. A. Gross, J. Viba, M. Cerpinska, Unveiling ice friction and aerodynamic drag at the initial stage of sliding on ice: Faster sliding in winter sports, *Tribology International* 160 (2021) 106967. doi:10.1016/j.triboint.2021.106967.
- [11] E. Lozowski, K. Szilder, L. Poirier, A bobsleigh ice friction model, *International Journal of Offshore and Polar Engineering* (2013).
- [12] M. Mössner, M. Hasler, K. Schindelwig, P. Kaps, W. Nachbauer, An approximate simulation model for initial luge track design, *Journal of Biomechanics* 44 (2011) 892–896. doi:10.1016/j.jbiomech.2010.12.001.
- [13] R. W. Liefferink, F.-C. Hsia, B. Weber, D. Bonn, Friction on ice: How temperature, pressure, and speed control the slipperiness of ice, *Physical Review X* 11 (2021) 453. doi:10.1103/PhysRevX.11.011025.
- [14] Velkavrh, Lungevičs, Jansons, Klien, Voyer, Ausserer, The influence of isotropic surface roughness of steel sliders on ice friction under different testing conditions, *Lubricants* 7 (2019) 106. doi:10.3390/lubricants7120106.
- [15] G. S. Rempfler, Entwicklung eines Bobsimulators, Ph.D. thesis, ETH Zurich, 2015. doi:10.3929/ETHZ-A-010474676.
- [16] G. S. Rempfler, C. Glocker, A bobsleigh simulator software, *Multibody System Dynamics* 36 (2016) 257–278. doi:10.1007/s11044-015-9450-2.
- [17] P. Arnold, Analyse und Konzeption von Bobfahrwerken, Thesis, 2013.
- [18] M. Scherge, The kreisel in winterberg – speed and acceleration, *Gliding* 2021 (2021).
- [19] F. Braghin, M. Donzelli, S. Melzi, E. Sabbioni, A driver model of a two-man bobsleigh, *Sports Engineering* 13 (2011) 181–193. doi:10.1007/s12283-011-0066-3.
- [20] F. Braghin, F. Cheli, M. Donzelli, S. Melzi, E. Sabbioni, Multi-body model of a bobsleigh: comparison with experimental data, *Multibody System Dynamics* 25 (2011) 185–201. doi:10.1007/s11044-010-9218-7.
- [21] J. von Schleinitz, L. Wörle, M. Graf, A. Schröder, W. Trutschnig, Analysis of race car drivers’ pedal interactions by means of supervised learning, in: 2019 IEEE Intelligent Transportation Systems Conference (ITSC), 2019, pp. 4152–4157. doi:10.1109/ITSC.2019.8917120.
- [22] L. Wörle, Objective Criteria for the Driving Style of Race Car Drivers, Doctoral thesis, TU Graz, Graz, 2020.
- [23] J. von Schleinitz, M. Graf, W. Trutschnig, A. Schröder, Vasp: An autoencoder-based approach for multivariate anomaly detection and robust time series prediction with application in motorsport, *Engineering Applications of Artificial Intelligence* 104 (2021) 104354. doi:10.1016/j.engappai.2021.104354.
- [24] T. Schwarzhuber, J. von Schleinitz, H. Geiser, M. Graf, A. Eichberger, Drivers’ controlled stimuli in

- nonlinear vehicle dynamics driving simulation, in: Proceedings of the Driving Simulation Conference 2020, Driving Simulation Association, 2020, p. 45.
- [25] T. Schwarzhuber, L. Wörle, M. Graf, A. Eichberger, Validity quantification of driver-in-the-loop simulation in motorsport, Fisita F2020 (waiting for Publication) 2020 (2020).
 - [26] J. von Schleinitz, T. Schwarzhuber, L. Wörle, M. Graf, A. Eichberger, W. Trutschig, A. Schröder, Race driver evaluation at a driving simulator using a physical model and a machine learning approach, waiting for publication - submitted to Vehicle System Dynamics 2021 (2021).
 - [27] C. Gong, C. W. Phillips, E. Rogers, S. R. Turnock, Analysis of performance indices for simulated skeleton descents, Procedia Engineering 147 (2016) 712–717. doi:10.1016/j.proeng.2016.06.253.
 - [28] Y. L. Zhang, M. Hubbard, R. K. Huffman, Optimum control of bobsled steering, Journal of Optimization Theory and Applications 85 (1995) 1–19. URL: <https://doi.org/10.1007/BF02192297>. doi:10.1007/BF02192297.
 - [29] J. Albery, C. Carstensen, S. A. Funken, R. Klose, Matlab implementation of the finite element method in elasticity, Computing 69 (2002) 239–263. URL: [GotoISI://WOS:000180161600004](https://www.wos.com/000180161600004). doi:10.1007/s00607-002-1459-8.
 - [30] A. Schröder, H. Blum, Projective sor-procedures for signorini problems, AIP Conference Proceedings 1048 2008 (2008) 474–477. doi:10.1063/1.2990965.
 - [31] P. Riekert, T. Schunck, Zur fahrmechanik des gummbereiften kraftfahrzeugs, Ingenieur-Archiv 11 (1940) 210–224.
 - [32] H. B. Pacejka, E. Bakker, The magic formula tyre model, Vehicle System Dynamics 21 (1992) 1–18. doi:10.1080/00423119208969994.
 - [33] F. J. Bello-Millán, T. Mäkelä, L. Parras, C. Del Pino, C. Ferrera, Experimental study on ahmed’s body drag coefficient for different yaw angles, Journal of Wind Engineering and Industrial Aerodynamics 157 (2016) 140–144. doi:10.1016/j.jweia.2016.08.005.
 - [34] A. Sciacchitano, P. Pattnaik, Near wake analysis of a two-man bobsleigh scaled model, Proceedings 2 (2018) 319. doi:10.3390/proceedings2060319.
 - [35] E. Jansons, M. Irbe, K. A. Gross, Influence of weather conditions on sliding over ice at a push-start training facility, Biotribology 25 (2021) 100152. doi:10.1016/j.biotri.2020.100152.